Significant effect of interfacial spin moments in ferromagnet-semiconductor heterojunctions on spin transport in a semiconductor

T. Naito,[1] R. Nishimura,[1] M. Yamada,[2,3] A. Masago,[3] Y. Shiratsuchi,[4,3,5] Y. Wagatsuma,[6] K. Sawano,[6] R. Nakatani,[4,3,5] T. Oguchi,[3,5] and K. Hamaya[3,1,5,*]

[1]*Department of Systems Innovation, Graduate School of Engineering Science, Osaka University, 1-3 Machikaneyama, Toyonaka 560-8531, Japan*

[2]*PRESTO, Japan Science and Technology Agency, 4-1-8 Honcho, Kawaguchi, Saitama 332-0012, Japan*

[3]*Center for Spintronics Research Network, Graduate School of Engineering Science, Osaka University, 1-3 Machikaneyama, Toyonaka 560-8531, Japan*

[4]*Department of Materials Science and Engineering, Graduate School of Engineering, Osaka University, 2-1 Yamadaoka, Suita 565-0871, Japan*

[5]*Division of Spintronics Research Network, Institute for Open and Transdisciplinary Research Initiatives, Osaka University, Yamadaoka 2-1, Suita, Osaka 565-0871, Japan*

[6]*Advanced Research Laboratories, Tokyo City University, 8-15-1 Todoroki, Tokyo 158-0082, Japan*

(Received 10 February 2022; revised 25 April 2022; accepted 27 April 2022; published 13 May 2022)

Using controlled ferromagnet (FM) -semiconductor (SC) interfaces in SC-based lateral spin-valve (LSV) devices, we experimentally study the effect of interfacial spin moments in FM–SC heterojunctions on spin transport in SC. First-principles calculations predict that the spin moment of FM–SC junctions can be artificially reduced by inserting 3*d* transition metal V, Cr, or Cu atomic layers between FM and SC. When all-epitaxial FM–SC Schottky-tunnel contacts with a 0.4–0.5-nm-thick V, Cr, or Cu interfacial layer are formed, we find that the spin signals in FM–SC LSV devices are significantly decreased at 8 K. When we increase the interfacial spin moment by inserting an ∼0.3-nm-thick Co layer between FM and SC, the spin signals at 8 K are significantly enhanced again. From these experiments, we conclude that the interfacial spin moments at FM–SC interfaces are one of the important factors to achieve large spin signals even in SC-based spintronic devices.

DOI: 10.1103/PhysRevB.105.195308

I. INTRODUCTION

Spin-dependent transport properties have been explored in many vertically stacked structures with ferromagnetic metal (FM) –insulator [1–4] and/or FM–nonmagnetic metal (NM) [5–8] interfaces such as magnetic tunnel junctions (MTJs) and current perpendicular to the plane (CPP) giant magnetoresistance (GMR) devices. For improving tunneling magnetoresistance (TMR) and GMR effects, in particular, a few atomic layers of a transition metal (TM) have been inserted between the FM electrode and the insulator layer [9–16] or between the FM electrode and the NM layer [17,18]. These inserted atomic layers of TM resulted mainly in the modulation of the electron-band symmetry matching and the spin-dependent scattering at the interface [9–12]. In addition, despite the variation in a few atomic layers, interfacial spin moments can be changed [11,13,14] and atomic interdiffusion can be suppressed [15,16], causing a significant influence on the TMR ratios.

For semiconductor (SC) -based spintronic devices such as FM–SC–FM structures [19–24], however, the interface effect on the spin-dependent transport properties has not precisely been understood because of the more complicated situations as follows. First, in laterally configured FM–SC–FM devices, spin relaxation during the diffusive transport in SC channels should be taken into account as well as spin injection/detection through the FM–SC interfaces. Second, the spin injection/detection efficiency depends on the width of the Schottky-tunnel barrier and the interface resistance of the FM–SC heterojunctions, and the interdiffusion between FM and SC atoms makes it difficult to control interfacial atomic layers [25–27], which degrades interfacial spin polarization. Interdiffusion between FM and SC atoms can significantly affect the spin injection/detection efficiency by the applied bias voltage [28]. Finally, due to the large nonlinear electric transport at the FM–SC junctions with a tunnel barrier, the spin detection efficiency at the FM–SC contacts is strongly influenced by the bias voltage [29,30]. For these reasons, it is generally difficult to understand the role of interface properties on the spin-dependent transport in laterally configured FM–SC–FM spintronic devices.

In these aforementioned situations in SC-based spintronic devices, we have so far examined the spin transport properties in one of the SC materials, germanium (Ge), as a spin transport layer in lateral spin-valve (LSV) devices [24]. First, almost all the spin relaxation phenomena in *n*-Ge have been clarified via temperature-dependent spin transport measurements [24,31–34], together with the comparisons of the experimental data and theories [35–37]. Second, since

*hamaya.kohei.es@osaka-u.ac.jp

high-quality FM–Ge heterostructures without atomic interdiffusion have been developed [38,39], the influence of degradation of the FM materials on the spin transport properties can be minimized. Finally, owing to the phosphorus (P) δ-doping technique to control the width of the FM/Ge Schottky-tunnel barrier [24,40], current density–voltage ($|J| - V$) characteristics of the FM/Ge contacts show the tunnel conduction. Therefore, if the resistivity of the *n*-Ge and the interface resistance of the FM/Ge Schottky-tunnel junctions are constant for each device, the effect of interfacial properties on the spin transport in FM–Ge–FM LSV devices can be explored to verify the role of FM–SC interfaces.

In this article, using controlled FM–SC interfaces in FM–SC–FM LSV devices, we experimentally study the effect of interfacial spin moments at the FM–SC interfaces on the spin transport in SC. First-principles calculations predict that the spin moment at the FM–SC interface can be artificially reduced by inserting 3*d* TM (V, Cr, or Cu) atomic layers between FM and SC. When all-epitaxial FM–SC interfaces with a 0.4–0.5-nm-thick V, Cr, or Cu layer are formed, we find that the spin signals in the LSV devices are significantly reduced even at 8 K. When we increase the interfacial spin moment by inserting an ∼0.3-nm-thick Co at the FM–SC interface, the spin signals are significantly enhanced again. From these experiments, we conclude that the interfacial spin moments at FM–SC interfaces are one of the important factors to achieve large spin signals in SC-based spintronic devices.

II. THEORETICAL PREDICTION

First, we theoretically estimate the spin moments of the FM–SC interfaces when 3*d* TM (V, Cr, or Cu) atomic layers are inserted. For comparison with experiments, the FM and SC layers in the calculation are considered to be Co_2FeSi (CFS) and Ge, respectively, where the Ge(111) surface is terminated by five atomic layers of Fe, as shown in Refs. [38,39]. Also, we used a model of the CFS–TM–Fe structure, in which 1.5 unit cells of CFS, three TM atoms, and three Fe atoms were stacked along the [111] direction for Ge, as shown in Fig. 1. The light gray, the magenta, the dark gray, and the black spheres indicate Fe, TM, Co, and Si, respectively. Here when we used 4.5 unit cells of CFS for the calculations, there was no significant difference in the results (not shown here). The lattice constants of the supercell, *a* and *c*, were 3.99 Å and 9.75 Å on the basis of the experimental values. The spin moments in these systems were calculated by a first-principles calculations package of Akai-KKR [41], employing Korringa-Kohn-Rostoker (KKR) Green's function method [42,43] applied with the Moruzzi-Janak-Wiliams (MJW) exchange-correlation potential [44]. The first Brillouin zone was integrated using 868 *k*-points.

Figure 1 shows the calculated spin moment of the atom on each layer, where the red closed circles, the green open boxes, and the blue open circles indicate CFS–V–Fe, CFS–Cr–Fe, and CFS–Cu–Fe systems, respectively. Here, the lateral axis of this figure means the atoms that are arranged according to the atomic configuration of the model structure along the [111] direction of Ge. These atoms are contained one by one in the unit cell of each single layer. In this figure, we can see a significant difference in the spin moments at the Fe

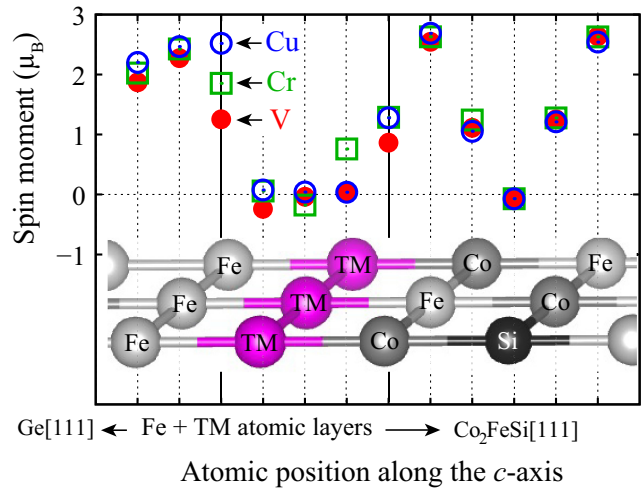

FIG. 1. Calculated spin moments of each atom along the Ge[111] direction and a schematic of a part of the stacked supercell, Fe (3 atoms)/TM (3 atoms)/Co_2FeSi.

atom next to the 3*d* TM (V, Cr, or Cu) (see arrows). Since the change in the magnitude of the spin moments depends on the atomic numbers of V, Cr, and Cu, the TM atoms affect the Fe atom through the following three steps: (1) the 3*d* spin majority state of the TM atom becomes more stable as its electron configuration approaches the half-filled configuration that is the closed shell structure within the majority spin state, (2) the stable 3*d* state of the TM atom localizes and suppresses the hybridization with the 3*d* state of the Fe atom, and (3) the high-spin state is formed due to the half-filled electron configuration (Hund's rule) of the Fe-3*d* state [45].

In the structure considered here, the spin moments in the TM layer are also influenced by the adjacent atoms. Although V is generally a paramagnetic element, two of three V atoms in this calculation show a ferromagnetic order with a very small spin moment. Since Cr is known as an antiferromagnetic element, the negative spin moment in the central Cr atom is nearly equal to the positive one in the Cr atom next to the Fe atom. However, the value of the spin moment next to the Co atom is relatively large even for Cr. For a nonmagnetic element Cu, on the other hand, the spin moments in the three atoms are the smallest value in these systems, which agrees well with a previous paper [46]. Because the Cu-3*d* state is the closed shell configuration, the Cu-3*d* considered here is very stable and localized.

From these theoretical predictions, the spin moments of the CFS–TM–Fe systems on top of the Ge (111) can be intentionally reduced. By using an insertion of TM atomic layers in experiments, we can explore the effect of the interfacial spin moments on the spin transport in *n*-Ge-based LSV devices with CFS–TM–Fe/Ge Schottky-tunnel contacts.

III. RESULTS

A. Formation of FM–TM–SC interfaces

To verify the theoretical predictions shown in Sec. II, FM–SC heterostructures with a 3*d* TM insertion layer were formed by low-temperature molecular beam epitaxy (MBE)

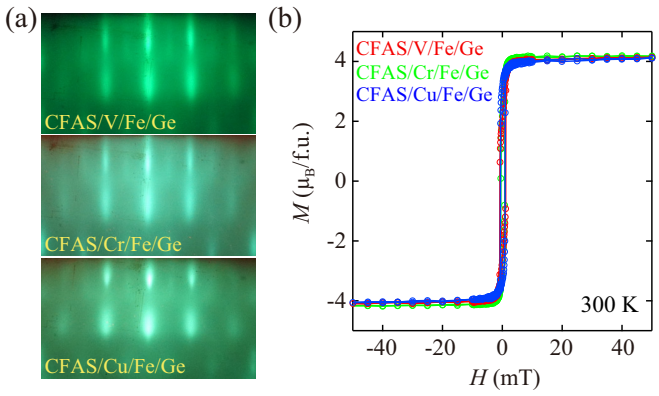

FIG. 2. (a) *in situ* RHEED patterns of the CFAS surface on the V, Cr, and Cu insertion layers on Fe-terminated Ge(111). (b) $M-H$ curves at 300 K for the 7–8-nm-thick CFAS films on the TM(V, Cr, or Cu)/Fe/Ge(111)/Si(111).

[24,31], where the FM and SC layers are $Co_2FeAl_{0.5}Si_{0.5}$ (CFAS) and Ge, respectively, and the surface of the Ge layer was terminated by an ∼0.4-nm-thick Fe layer to suppress the outdiffusion of Ge atoms into CFAS [38]. Here, given the prediction in Sec. II, we used a 0.4–0.5-nm-thick V, Cr, or Cu layer as a TM layer. Figure 2(a) shows *in situ* reflection high energy electron diffraction (RHEED) patterns of 7–8-nm-thick CFAS layers grown on V, Cr, and Cu insertion layers on top of the Fe-terminated Ge(111) on Si(111) [38]. Clear streak patterns for all the three FM–TM–Fe-terminated Ge(111) are seen, indicating that two-dimensional epitaxial growth of the CFAS layer is guaranteed even on top of the very thin TM layers.

To evaluate magnetic properties of the CFAS layers, field-dependent magnetization (M–H) curves are measured by vibrating sample magnetometer (VSM) at 300 K in Fig. 2(b). The saturation magnetization (M_S) is 4.1, 4.2, and 4.2 μ_B/formula unit (f.u.) for the CFAS/V/Fe/Ge, CFAS/Cr/Fe/Ge, and CFAS/Cu/Fe/Ge structures, respectively. In addition to this, the coercivity (H_C) is within 0.6–1 mT in all the structures. These values of M_S and H_C are almost the same and consistent with those of the CFAS/Fe/Ge or CFAS/Ge structures in our previous works [31,39]. Thus the quality of the CFAS layers is also guaranteed as high-performance FM contacts, shown in Ref. [38].

B. Spin transport signals

To examine the influence of the presence of the TM inserted layers at the FM–SC interface on spin injection/detection in FM–SC–FM structures, we prepared LSV devices with the controlled CFAS–TM–Fe/Ge Schottky-tunnel contacts on Si(111). The LSV structures are schematically illustrated in Fig. 3(a). An ∼140-nm-thick n-Ge ($n = 5.1 \times 10^{18}$ cm^{-3} at 300 K) spin-transport layer was grown on an undoped Ge(∼100 nm)/Si(111) substrate, where the undoped Ge buffer layer was grown by two-step growth technique [47]. To obtain a small rectification of the electrical transport properties via the CFAS/Ge interface, we inserted two δ-doped P/Si layers [24,40], as shown in the left of Fig. 3(a). On top of the Ge(111) surface, the CFAS/V/Fe

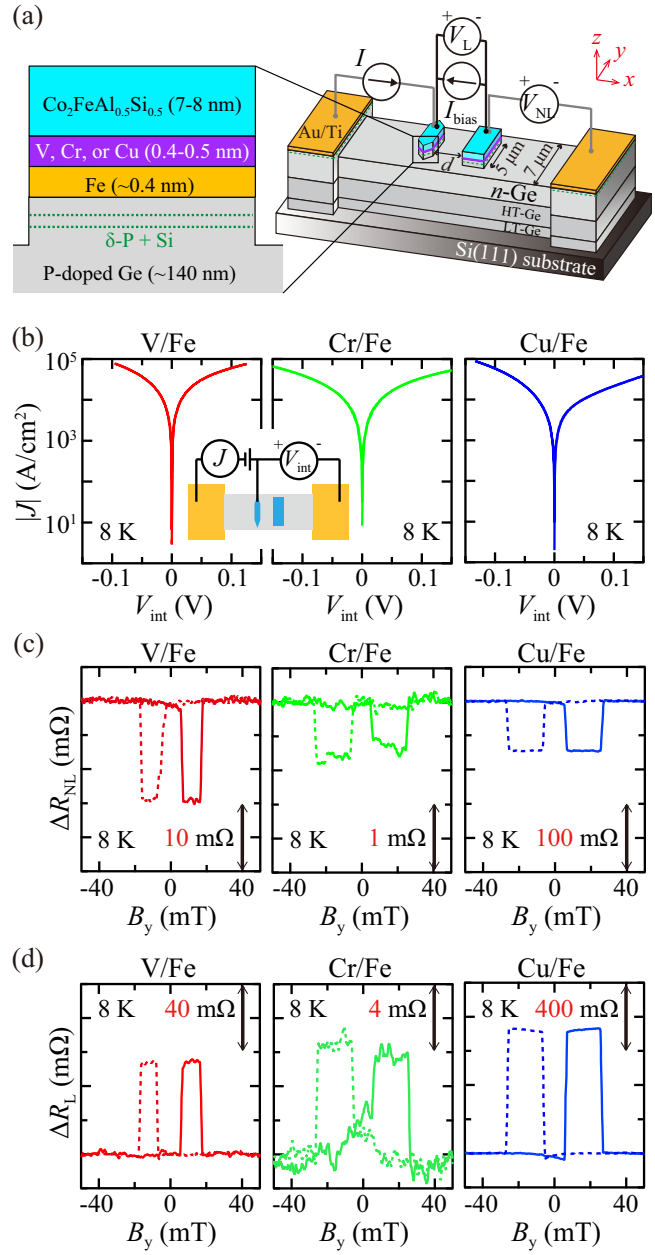

FIG. 3. (a) Schematic of a fabricated LSV device and terminal configurations of four-terminal nonlocal and two-terminal local magnetoresistance measurements. A cross section of the CFAS/TM/Fe/Ge contact is enlarged on the left. (b) $|J|$-V_{int} characteristics for the Schottky-tunnel contacts (contact area ∼ 2.0 μm^2) measured in the three-terminal configuration (inset) at 8 K for devices with V/Fe, Cr/Fe, and Cu/Fe insertion layers. (c) Nonlocal and (d) local magnetoresistance curves for each device at 8 K.

(V/Fe), CFAS/Cr/Fe (Cr/Fe), or CFAS/Cu/Fe (Cu/Fe) structures were grown by MBE as shown in Fig. 2(a). Each heterostructure was patterned into the channel structure with a channel width of 7.0 μm and, then, two FM contacts were fabricated on the remaining structure. The size of the spin injector (detector) contact and edge-to-edge distances (d) between the contacts were designed to be 0.4 × 5.0 μm^2 (1.0 × 5.0 μm^2)

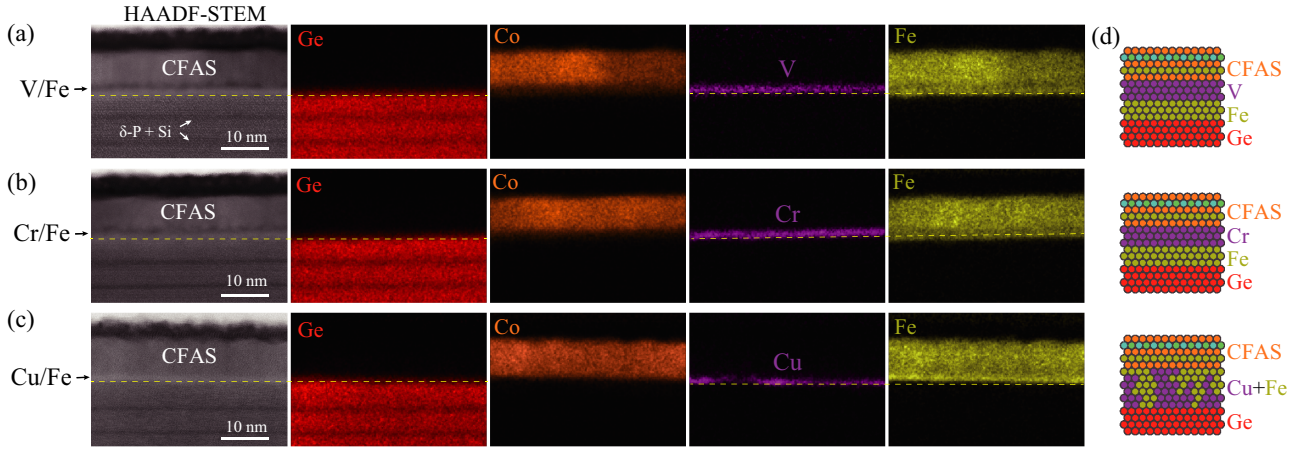

FIG. 4. HAADF STEM images and EDX maps near the CFAS/TM/Fe/Ge interfaces in LSV devices for (a) V/Fe, (b) Cr/Fe, and (c) Cu/Fe. (d) Schematics of the interfacial structure expected from the structural analyses for each device.

and 0.4–0.7 μm. The detailed fabrication process of the LSV devices is presented in our previous work [28].

Figure 3(b) shows representative current density (J)–interfacial voltage ($V_{\rm int}$) characteristics of the Schottky-tunnel contacts at 8 K, measured in the three-terminal configuration shown in the inset. For the devices with the V/Fe or Cr/Fe insertion layer, $|J| - V_{\rm int}$ curves clearly show almost no rectifying behavior. Although the magnitude of J in the reverse bias condition ($V_{\rm int} \leqslant 0$) is higher than that in the forward bias one ($V_{\rm int} \geqslant 0$) for the device with the Cu/Fe insertion layer, a marked Schottky diode characteristic cannot be seen. Thus, for all the devices, the tunnel conduction of electrons dominates the $|J| - V_{\rm int}$ characteristics even at 8 K.

Using these spin injector and detector contacts, we perform four-terminal nonlocal and two-terminal local magnetoresistance measurements at 8 K, where the nonlocal and local spin signals are defined as $\Delta R_{\rm NL} = \Delta V_{\rm NL}/I$ and $\Delta R_{\rm L} = \Delta V_{\rm L}/I_{\rm bias}$, respectively. Here the values of $\Delta V_{\rm NL}$ and $\Delta V_{\rm L}$ are nonlocal and local voltage changes during the measurements. Figures 3(c) and 3(d) display representative $\Delta R_{\rm NL}$ and $\Delta R_{\rm L}$ as a function of magnetic fields ($B_{\rm y}$) at 8 K, respectively. For all the devices with TM layers, both nonlocal and local spin signals are clearly observed. In addition, nonlocal Hanle curves were also observed by applying B_z at 8 K (not shown here). Thus we conclude that spin transport in n-Ge is observed at 8 K even for LSV devices with TM layers. Notably, the magnitude of $\Delta R_{\rm NL}$ and $\Delta R_{\rm L}$ is greatly different despite the same magnetic property of the CFAS spin injector and detector material, as shown in Fig. 2. Prior to the discussion on the correlation between the magnitude of $\Delta R_{\rm NL}$ and $\Delta R_{\rm L}$ and the interfacial spin moments in Sec. II, we should confirm the interface quality for these three devices. The detailed structural characterizations are conducted in the next subsection C.

C. Structural analyses of FM–SC interfaces

Using high angle annular dark field (HAADF) scanning transmission electron microscopy (STEM) imaging and energy-dispersive x-ray spectroscopy (EDX) mapping, we perform a structural analysis of the interfaces of the spin injector or detector contact. Figures 4(a)– 4(c) show the HAADF-STEM images and elemental EDX maps for the CFAS/V/Fe, CFAS/Cr/Fe, and CFAS/Cu/Fe structures in the LSV devices used in the previous subsection B. In the HAADF-STEM images for the CFAS/V/Fe and CFAS/Cr/Fe structures, we find similar contrast changes to dark regions on top of the Ge in Figs. 4(a) and 4(b), respectively. From the related EDX maps, we can determine the dark contrast regions as the inserted V or Cr layer. It should be noted that the V or Cr layer exists on top of the Fe layer on the Ge surface (see yellow dashed lines). Thus the all-epitaxial CFAS/V/Fe/Ge and CFAS/Cr/Fe/Ge structures are formed expectedly. In these structures, we also observe no outdiffusion of Ge atoms into the CFAS layer, similar to our previous work [38].

In Fig. 4(c), on the other hand, the contrast of the HAADF-STEM image for the CFAS/Cu/Fe structure is evidently different from these for the CFAS/V/Fe and CFAS/Cr/Fe structures. We note that, in the EDX map for Cu, the layer structure is not maintained unexpectedly. In addition to this, the distribution of Fe is overlapped on the region of Cu. According to the literature [48], bcc-Cu–Fe systems are not stable, and Fe and Cu are almost insoluble at room temperature. On the other hand, some literature reported on interdiffusion of Cu and Fe atoms near the heterointerfaces [49,50]. From these facts, the all-epitaxial CFAS/Cu/Fe/Ge stack is not perfectly formed but is changed to the epitaxial CFAS/(CuFe) mixed layer/Ge during the growth. Given these complicated situations, we summarize the results of structural analyses as simple schematics in Fig. 4(d). To discuss the influence of the spin moment near the FM–SC interface on the spin-transport properties, we should reconsider the correlation between the detailed structures near the interface in Fig. 4 and the theoretical prediction in Fig. 1.

IV. DISCUSSION

In this section, we discuss the correlation between the interfacial spin moment and the spin transport in SC through FM–SC interfaces. First, to compare the spin-transport properties, we also analyze the spin signals for the three LSV devices with the CFAS/V/Fe, CFAS/Cr/Fe, and CFAS/(CuFe)

TABLE I. Summary of nonlocal ($|\Delta R_{NL}|$) and local ($|\Delta R_L|$) spin signals at 8 K in LSV devices with various d and FM/SC interfaces. $P_{inj/det}$ estimated from $|\Delta R_{NL}|$ at 8 K and the interfacial average spin moments (M) calculated in Fig. 1 for V and Cr layers and recalculated for CuFe mixed layer are shown, together with those for only-Fe-inserted device in Ref. [38].

Stacking structure on Ge(111)	d (μm)	$\|\Delta R_{NL}\|$ (mΩ)	$\|\Delta R_L\|$ (mΩ)	$P_{inj/det}$ (%)	M (μ_B)
CFAS/V(∼0.5 nm)/Fe(∼0.4 nm)	0.4	12.5	25.5	2.3	−0.08
	0.5	14.6	54.2	2.5	
	0.7	10.0	20.1	2.5	
CFAS/Cr(∼0.4 nm)/Fe(∼0.4 nm)	0.5	0.77	8.8	0.6	0.21
	0.6	0.72	6.2	0.6	
	0.7	0.69	6.1	0.6	
CFAS/CuFe(0.9 ∼ 1 nm)	0.4	82.9	732.3	4.4	1.27
	0.5	72.6	723.8	4.2	
	0.6	65.1	686.1	4.2	
CFAS/Fe(∼0.7 nm) in Ref. [38]	0.45	468.8	1207.7	24	2.51

contacts, as representatively shown in Figs. 3(c) and 3(d). In general, the spin injection/detection efficiency ($P_{inj/det}$) can be estimated from the value of ΔR_{NL} in four-terminal nonlocal magnetoresistance measurements as follows [51]:

$$|\Delta R_{NL}| = \frac{P_{inj/det}^2 \rho_N \lambda_N}{S} \exp\left(-\frac{d}{\lambda_N}\right), \quad (1)$$

where ρ_N, λ_N, and S are the resistivity (2.4–3.2 mΩ cm at 8 K), the spin diffusion length (∼1.1 μm at 8 K estimated from Hanle curve fitting [19]), and the cross sectional area (0.54–0.86 μm^2) of the SC layer, respectively. In Table I, we summarize the values of $|\Delta R_{NL}|$, $|\Delta R_L|$, and $P_{inj/det}$ estimated from Eq. (1) at 8 K for the LSV devices with the CFAS/V/Fe, CFAS/Cr/Fe, and CFAS/(CuFe) contacts, together with the expected average spin moments M in first-principles calculations in Fig. 1. Here we replace the previous indication of CFAS/Cu/Fe with the real situation of CFAS/(CuFe). For reference, the data for an LSV with the CFAS/Fe (∼0.7 nm) contacts at 8 K in Ref. [38] are shown together.

First, we find that the estimated values of $|\Delta R_L|$ are always greater than those of $|\Delta R_{NL}|$ at 8 K. This feature is attributed to the spin detection efficiency enhancement at an FM–Ge detector contact by a positive bias voltage [29,30] and/or the enhancement in the spin transport length in the Ge layer by an electric field [52]. Given the above situations, we estimated $P_{inj/det}$ only from $|\Delta R_{NL}|$. Notably, we observe that the magnitude of $|\Delta R_{NL}|$ and $|\Delta R_L|$ for the CFAS/Cr/Fe is three orders of magnitude smaller than those for the CFAS/Fe in Ref. [38]. Only an ∼0.4-nm-thick Cr layer near the CFAS–Fe interface significantly affects the spin injection, transport, and detection in n-Ge even at 8 K. The similar feature is also observed for the case of the CFAS/V/Fe. After the recalculation for the M in the CFAS/CuFe/Ge structure, the M value becomes larger than that in the CFAS/Cu/Fe/Ge structure because of the presence of the Fe atoms in the whole interface region. When we focus on the magnitude relationship of $P_{inj/det}$ at 8 K, it seems that they are roughly related to the magnitude of M. This fact implies that the interfacial magnetic properties in FM–SC–FM structures influence strongly the spin-transport properties even at low temperatures.

To check the aforementioned hypothesis on the influence of the interfacial spin moments or magnetic properties, we fabricated again the LSV device with CFAS (∼8 nm)/Co (∼0.3 nm)/Fe (∼0.3 nm) contacts, where the Co layer was also grown by the low-temperature MBE technique. After the three atomic layers of Co (∼0.3 nm) are inserted between CFAS and Fe, the M value is theoretically estimated to be ∼1.8 μ_B, comparable to that in the case of the Fe layer insertion, from the first-principles calculations. From the HAADF-STEM image and EDX elemental maps, the inserted Co layer did not exist beneath the Fe layer on the Ge surface (not shown here). Thus the all-epitaxial CFAS/Co/Fe/Ge structure is formed expectedly to check the effect of the increase in the M on the spin-transport properties. Figures 5(a) and 5(b) show ΔR_{NL} and ΔR_L as a function of B_y at 8 K, respectively, for an LSV device with $d = 0.45$ μm. Notably, the magnitude of ΔR_{NL} and ΔR_L is greatly enhanced, indicating that the spin signals for the CFAS/Co/Fe contacts are much larger than those for the previous CFAS/V/Fe, CFAS/Cr/Fe, and CFAS/CuFe contacts in Table I. As a result, we have clarified that the spin moments at FM–SC interfaces significantly affect the spin transport in SC channels even at low temperature.

Finally, we comment on the mechanism of the significant effect of interfacial spin moments at FM–SC interfaces on the spin transport in SC. Recent studies have shown the large impact of high-quality Co-based Heusler-alloy FM

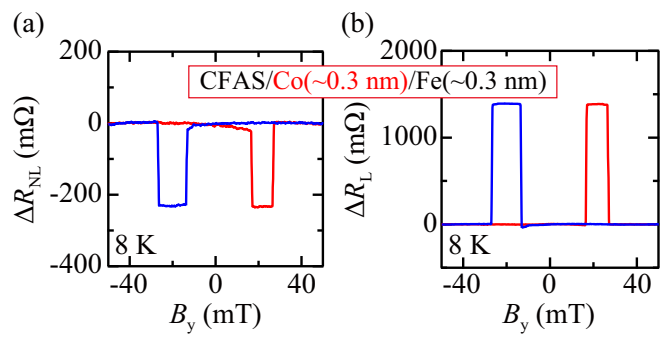

FIG. 5. (a) Nonlocal and (b) local magnetoresistance curves for an LSV device with CFAS(∼8 nm)/Co(∼0.3 nm)/Fe(∼0.3 nm)/Ge contacts, measured at $I_{bias} = -0.7$ mA and at 8 K.

spin injector and detector on the spin transport in *n*-Ge [24,38,39,53]. Despite the insertion of an ∼0.7-nm-thick Fe layer between FM and Ge, highly efficient spin injection and detection through the FM/Fe/Ge(111) interfaces have been observed [38,39,53]. Given these situations, we infer that an electron-band symmetry matching for the efficient injection of spin-polarized electrons into the conduction band of Ge occurs along ⟨111⟩ directions [38]. If there was the V/Fe, Cr/Fe, or CuFe interface between CFAS and Ge along ⟨111⟩ directions, the electron-band symmetry matching for the efficient injection of spin-polarized electrons may be influenced. However, since the spin-transport properties shown in Table I and in Fig. 5 are strongly related to the magnitude of M, we should consider another mechanism on the basis of the *s*-*d* exchange interaction between conduction *s* electrons and localized *d* electrons at the FM–SC interface, as recently discussed in MTJs [54]. When M is significantly small, the local *d* spins fluctuate at finite temperature. Even at 8 K, a small M indicates large fluctuation of the *d* spins. As a consequence of the above *s*-*d* exchange interaction between the highly spin-polarized electrons from CFAS and the largely fluctuating *d* electrons at the V/Fe, Cr/Fe, or CuFe interfaces, spin-flip scattering at the interface can be induced, leading to the reduction in $P_{\mathrm{inj/det}}$ in FM–SC–FM structures. In this study, the crucial role of the interfacial *s*-*d* exchange interaction may be detected even in SC-based spintronic device structures.

V. CONCLUSION

Using controlled FM–SC interfaces in SC-based LSV devices, we experimentally study the effect of interfacial spin moments at FM–SC interfaces on the spin transport in SC. First-principles calculations predict that the spin moment at an FM–SC interface can be artificially reduced by inserting V, Cr, or Cu atomic layers between FM and SC. When all-epitaxial FM–SC interfaces with a 0.4–0.5-nm-thick V, Cr, or Cu layer were formed, we found that the spin signals in FM–SC LSV devices are significantly decreased even at 8 K. When we increased the interfacial spin moment by inserting ∼0.3-nm-thick Co between FM and SC, the spin signals were significantly enhanced again. From these experiments, we conclude that the interfacial spin moments at FM–SC interfaces are one of the important factors to achieve large spin signals in SC-based spintronic devices.

ACKNOWLEDGMENTS

This work was partly supported by JSPS KAKENHI (Grants No. 19H05616, No. 19H02175, No. 21H05000, and No. 21K18719), JST PRESTO (Grant No. JPMJPR20BA), Iketani Science and Technology Foundation, The Murata Science Foundation, and the Spintronics Research Network of Japan (Spin-RNJ). T.N. acknowledges JSPS Research Fellowship for Young Scientists.

[1] S. S. P. Parkin, C. Kaiser, A. Panchula, P. M. Rice, B. Hughes, M. Samant, and S.-H. Yang, Nat. Mater. **3**, 862 (2004).
[2] S. Yuasa, T. Nagahama, A. Fukushima, Y. Suzuki, and K. Ando, Nat. Mater. **3**, 868 (2004).
[3] S. Ikeda, K. Miura, H. Yamamoto, K. Mizunuma, H. D. Gan, M. Endo, S. Kanai, J. Hayakawa, F. Matsukura, and H. Ohno, Nat. Mater. **9**, 721 (2010).
[4] R. Shan, H. Sukegawa, W. H. Wang, M. Kodzuka, T. Furubayashi, T. Ohkubo, S. Mitani, K. Inomata, and K. Hono, Phys. Rev. Lett. **102**, 246601 (2009).
[5] M. N. Baibich, J. M. Broto, A. Fert, F. NguyenVan Dau, F. Petroff, P. Etienne, G. Creuzet, A. Friederich, and J. Chazelas, Phys. Rev. Lett. **61**, 2472 (1988).
[6] W. P. Pratt, Jr., S.-F. Lee, J. M. Slaughter, R. Loloee, P. A. Schroeder, and J. Bass, Phys. Rev. Lett. **66**, 3060 (1991).
[7] K. M. Schep, P. J. Kelly, and G. E. W. Bauer, Phys. Rev. Lett. **74**, 586 (1995).
[8] M. D. Stiles and D. R. Penn, Phys. Rev. B **61**, 3200 (2000).
[9] T. Nagahama, S. Yuasa, E. Tamura, and Y. Suzuki, Phys. Rev. Lett. **95**, 086602 (2005).
[10] F. Greullet, C. Tiusan, F. Montaigne, M. Hehn, D. Halley, O. Bengone, M. Bowen, and W. Weber, Phys. Rev. Lett. **99**, 187202 (2007).
[11] X. Feng, O. Bengone, M. Alouani, I. Rungger, and S. Sanvito, Phys. Rev. B **79**, 214432 (2009).
[12] Y. Wang, X. F. Han, and X.-G. Zhang, Appl. Phys. Lett. **93**, 172501 (2008).
[13] T. Saito, T. Katayama, T. Ishikawa, M. Yamamoto, D. Asakura, T. Koide, Y. Miura, and M. Shirai, Phys. Rev. B **81**, 144417 (2010).
[14] Y. Miura, K. Abe, and M. Shirai, Phys. Rev. B **83**, 214411 (2011).
[15] T. Yamamoto, T. Nozaki, K. Yakushiji, S. Tamaru, H. Kubota, A. Fukushima, and S. Yuasa, Acta Mater. **216**, 117097 (2021).
[16] K. Z. Suzuki, T. Ichinose, S. Iihama, R. Monma, and S. Mizukami, Appl. Phys. Lett. **118**, 172412 (2021).
[17] J. W. Jung, Y. Sakuraba, T. T. Sasaki, Y. Miura, and K. Hono, Appl. Phys. Lett. **108**, 102408 (2016).
[18] B. Büker, J. W. Jung, T. Sasaki, Y. Sakuraba, Y. Miura, T. Nakatani, A. Hütten, and K. Hono, Phys. Rev. B **103**, L140405 (2021).
[19] X. Lou, C. Adelmann, S. A. Crooker, E. S. Garlid, J. Zhang, K. S. M. Reddy, S. D. Flexner, C. J. Palmstrøm, and P. A. Crowell, Nat. Phys. **3**, 197 (2007).
[20] T. A. Peterson, S. J. Patel, C. C. Geppert, K. D. Christie, A. Rath, D. Pennachio, M. E. Flatté, P. M. Voyles, C. J. Palmstrøm, and P. A. Crowell, Phys. Rev. B **94**, 235309 (2016).
[21] I. Appelbaum, B. Huang, and D. J. Monsma, Nature (London) **447**, 295 (2007).
[22] R. Jansen, Nat. Mater. **11**, 400 (2012).
[23] Y. Zhou, W. Han, L.-T. Chang, F. Xiu, M. Wang, M. Oehme, I. A. Fischer, J. Schulze, R. K. Kawakami, and K. L. Wang, Phys. Rev. B **84**, 125323 (2011).
[24] K. Hamaya, Y. Fujita, M. Yamada, M. Kawano, S. Yamada, and K. Sawano, J. Phys. D: Appl. Phys. **51**, 393001 (2018).
[25] Y. Ebina, T. Akiho, H. Liu, M. Yamamoto, and T. Uemura, Appl. Phys. Lett. **104**, 172405 (2014).
[26] B. Kuerbanjiang, Y. Fujita, M. Yamada, S. Yamada, A. M. Sanchez, P. J. Hasnip, A. Ghasemi, D. Kepaptsoglou, G. Bell,

K. Sawano, K. Hamaya, and V. K. Lazarov, Phys. Rev. B **98**, 115304 (2018).
[27] A. Rath, C. Sivakumar, C. Sun, S. J. Patel, J. S. Jeong, J. Feng, G. Stecklein, P. A. Crowell, C. J. Palmstrøm, W. H. Butler, and P. M. Voyles, Phys. Rev. B **97**, 045304 (2018).
[28] Y. Fujita, M. Yamada, M. Tsukahara, T. Naito, S. Yamada, K. Sawano, and K. Hamaya, Phys. Rev. B **100**, 024431 (2019).
[29] R. Jansen, A. Spiesser, H. Saito, Y. Fujita, S. Yamada, K. Hamaya, and S. Yuasa, Phys. Rev. Appl. **10**, 064050 (2018).
[30] E. Fourneau, A. V. Silhanek, and N. D. Nguyen, Phys. Rev. Appl. **14**, 024020 (2020).
[31] Y. Fujita, M. Yamada, M. Tsukahara, T. Oka, S. Yamada, T. Kanashima, K. Sawano, and K. Hamaya, Phys. Rev. Appl. **8**, 014007 (2017).
[32] T. Naito, M. Yamada, S. Yamada, K. Sawano, and K. Hamaya, Phys. Rev. Appl. **13**, 054025 (2020).
[33] M. Yamada, Y. Fujita, M. Tsukahara, S. Yamada, K. Sawano, and K. Hamaya, Phys. Rev. B **95**, 161304(R) (2017).
[34] M. Yamada, T. Ueno, T. Naito, K. Sawano, and K. Hamaya, Phys. Rev. B **104**, 115301 (2021).
[35] P. Li, Y. Song, and H. Dery, Phys. Rev. B **86**, 085202 (2012).
[36] J-M. Tang, B. T. Collins, and M. E. Flatté, Phys. Rev. B **85**, 045202 (2012).
[37] Y. Song, O. Chalaev, and H. Dery, Phys. Rev. Lett. **113**, 167201 (2014).
[38] M. Yamada, F. Kuroda, M. Tsukahara, S. Yamada, T. Fukushima, K. Sawano, T. Oguchi, and K. Hamaya, NPG Asia Mater. **12**, 47 (2020).
[39] M. Yamada, Y. Shiratsuchi, H. Kambe, K. Kudo, S. Yamada, K. Sawano, R. Nakatani, and K. Hamaya, J. Appl. Phys. **129**, 183901 (2021).
[40] M. Yamada, K. Sawano, M. Uematsu, and K. M. Itoh, Appl. Phys. Lett. **107**, 132101 (2015).
[41] H. Akai, J. Phys. Soc. Jpn. **51**, 468 (1982).
[42] J. Korringa, Physica **13**, 392 (1947).
[43] W. Kohn and N. Rostoker, Phys. Rev. **94**, 1111 (1954).
[44] J. F. Janak, V. L. Moruzzi, and A. R. Williams, Phys. Rev. B **12**, 1257 (1975).
[45] A. Masago, H. Shinya, T. Fukushima, K. Sato, and H. Katayama-Yoshida, Appl. Phys. Express **14**, 091007 (2021).
[46] C. L. Fu, A. J. Freeman, and T. Oguchi, Phys. Rev. Lett. **54**, 2700 (1985).
[47] K. Sawano, Y. Hoshi, S. Kubo, K. Arimoto, J. Yamanaka, K. Nakagawa, K. Hamaya, M. Miyao, and Y. Shiraki, Thin Solid Films **613**, 24 (2016).
[48] Q. Chen and Z. Jin, Metall. Mater. Trans. A **26**, 417 (1995).
[49] V. Kuncser, W. Keune, U. von Hörsten, G. Schinteie, N. Stefan, P. Palade, and G. Filoti, Thin Solid Films **518**, 5981 (2010).
[50] M. Sun, A. Rauf, Y. Zhang, G. Sha, G. Peng, Z. Yu, C. Guo, Y. Fang, S. Lan, T. Feng, H. Hahn, and H. Gleiter, Mater. Res. Lett. **6**, 55 (2018).
[51] F. J. Jedema, H. B. Heersche, A. T. Filip, J. J. A. Baselmans, and B. J. van Wees, Nature (London) **416**, 713 (2002).
[52] Z. G. Yu and M. E. Flatté, Phys. Rev. B **66**, 235302 (2002).
[53] K. Kudo, M. Yamada, S. Honda, Y. Wagatsuma, S. Yamada, K. Sawano, and K. Hamaya, Appl. Phys. Lett. **118**, 162404 (2021).
[54] K. Masuda, T. Tadano, and Y. Miura, Phys. Rev. B **104**, L180403 (2021).